water

MDPI

Article

Slip Factor Correction in 1-D Performance Prediction Model for PaTs

Tommaso Capurso *, Michele Stefanizzi, Giuseppe Pascazio, Sergio Ranaldo, Sergio M. Camporeale, Bernardo Fortunato and Marco Torresi

Department of Mechanics, Mathematics and Management (DMMM), Polytechnic University of Bari, 70125 Bari, Italy; michele.stefanizzi@poliba.it (M.S.); giuseppe.pascazio@poliba.it (G.P.); sergio.ranaldo@poliba.it (S.R.); sergio.camporeale@poliba.it (S.M.C.); bernardo.fortunato@poliba.it (B.F.); marco.torresi@poliba.it (M.T.)

* Correspondence: tommaso.capurso@poliba.it; Tel.: +39-327-915-0352

Received: 29 December 2018; Accepted: 13 March 2019; Published: 19 March 2019

Abstract: In recent years, pumps operated as turbines (PaTs) have been gaining the interest of industry and academia. For instance, PaTs can be effectively used in micro hydropower plants (MHP) and water distribution systems (WDS). Therefore, further efforts are necessary to investigate their fluid dynamic behavior. Compared to conventional turbines, a lower number of blades is employed in PaTs, lowering their capability to correctly guide the flow, hence reducing the Euler's work; thus, the slip phenomenon cannot be neglected at the outlet section of the runner. In the first part of the paper, the slip phenomenon is numerically investigated on a simplified geometry, evidencing the dependency of the lack in guiding the flow on the number of blades. Then, a commercial double suction centrifugal pump, characterized by the same specific speed, is considered, evaluating the dependency of the slip on the flow rate. In the last part, a slip factor correlation is introduced based on those CFD simulations. It is shown how the inclusion of this parameter in a 1-D performance prediction model allows us to reduce the performance prediction errors with respect to experiments on a pump with a similar specific speed by 5.5% at design point, compared to no slip model, and by 8% at part-loads, rather than using Busemann and Stodola formulas.

Keywords: PaT; slip phenomenon; performance prediction; OpenFOAM; CFD

1. Introduction

The world electricity demand is increasing year by year, and the shift to renewable energy from fossil fuels is attracting many investments; at the same time, many financial resources are being spent to improve the efficiency of existing power plants and energy distribution systems. Hydropower, which comprises hydroelectric power plants and water distribution systems, is the main field where, in recent decades, pumps as turbines (PaTs) have been installed en masse. Many researchers strongly suggest the use of PaTs, i.e., conventional pumps used in reverse mode to recover energy from fluids subjected to a considerable pressure drop, as an alternative to throttling devices. PaTs are becoming more and more tempting because pumps are mass-produced, cheaper than conventional turbines and they cover a wide range of specific speeds and sizes.

Some technical reports by international pump manufacturers, like Sulzer and KSB, started to be published in the early 80s with Laux [1], who studied reverse-running multistage pumps as energy recovery turbines in oil supply systems; and Apfelbacher et al. [2] also studied the application of a PaT in a reduction pressure station in Aachen (Germany).

Large hydropower plants feed the national grid, whereas typical off-grid micro hydropower plants (MHP), in the range of 5–100 kW, are the most popular solutions for electrification among

rural communities [3]. In MHP, hydraulic turbines represent the critical technological component for energy production. Their cost significantly impacts the project budget. PaTs fulfill an important role in hydraulic pumped-storage plants to supply power peak demands; indeed, the oscillations of the power produced by renewable sources are going to promote the need for energy storage such as micro hydro, where the same machine needs to be operated both in pump mode and in turbine mode. Furthermore, PaTs can represent stand-alone small hydro systems in all those remote communities, where the grid connection is not economical and/or practically possible. In this case, PaTs can satisfy the energy demand by exploiting natural water sources.

Many works assess the installation of PaTs into Water Distribution Networks (WDNs) in order to save energy dissipated by pressure reducing valves (PRVs). PaTs found applications not only in the hydraulic sector, but also in other fields of the process engineering.

Nowadays, the prediction of the performance of a PaT is crucial in order to select the most suitable machine, starting from its geometric parameters and its specific speed, since pumps are not usually tested in turbine mode by manufacturers. Because of the lack of experimental data, considerable attempts have been made by several authors in the prediction of PaT performance, not only from a theoretical point of view, but also with experimental campaigns of pumps tested in reverse mode, as shown by Barbarelli et al. [4], Derakhshan and Nourbakhsh [5], Nautiyal et al. [6], Pugliese et al. [7], Rossi et al. [8], Singh and Nestmann [9], Shi et al. [10], Yang et al. [11], Tan and Engeda [12], Carravetta et al. [13].

Several models have been proposed for the prediction of the characteristic curve of a PaT. Some models, based on statistical and normalization approaches or artificial neural networks [14,15], are adopted when the geometric parameters of the runner are unknown [16], and they are useful to evaluate the flow rate and the head exploited by the PaTs running at their best efficiency point. At the same time, other models are based on theoretical approach as for the evaluation of the flow characteristics through the machine, as proposed by Barbarelli et al. [17], Gülich [18]. These are usually used by manufacturers, which have detailed information about their machines. The latter models currently show a lack of accuracy in the prediction of the characteristic curve, especially at part loads and over loads because of the simplification of the impeller channel and the volute geometry. For this reason, manufacturers need a tool that could support them not only to predict the turbine mode operation, but also to design ad hoc PaTs for specific applications by investigating more deeply the hydraulic behavior of their machines running in reverse mode.

Similarly to in centrifugal pumps, a slip phenomenon can also occur in turbines with a finite number of vanes, at the outlet section of the runner. As shown by Ventrone [19], the relative velocity vectors at the outlet of a centripetal turbine (e.g., Francis turbines and PaTs) are subject to a deflection with respect to the direction defined by the blade congruent angle (slip). Ventrone [19] and Shi et al. [20] justify the slip phenomenon by demonstrating the presence of fluid flow vorticity between the blades in planes orthogonal to the rotational axis. Thus, counter rotating vortices appear inside the impeller channels. This phenomenon shall be more evident in radial PaTs, where the number of blades is lower than in conventional turbines. In mixed axial-radial runners, additional dynamic effect should be taken into account.

The resulting flow deflection leads to an increase in the absolute tangential velocity and consequently a reduction of the extracted hydraulic energy with respect to the available one. Thus, in this work, the slip phenomenon in PaTs was studied in detail with the aim at focusing on the influence of the slip phenomenon on the performance prediction of PaTs. Regarding this aspect, the slip phenomenon is often neglected in prediction models and there are few works in the literature, which have investigated in detail the effect of the slip phenomenon in PaTs. Indeed, the evaluation of the slip effect is difficult and there are not many experimental correlations.

Differently from a previous work [21], herein the authors extended their investigations on the slip phenomenon at the outlet of PaTs. Arranging their work in three parts, the first, (Sections 2 and 3) and the last (Sections 5 and 6) parts being new. Moreover, additional details with respect to

the previous work are added. Initially, the reader is guided through a description of the problem (from a phenomenological point of view). Indeed, numerical investigations have been carried out on a simplified PaT runner geometry, designed according to potential flow solution, in order to study the slip phenomenon and be able to more easily describe the sources of the flow deflection (see Sections 2 and 3). In the second part, the work deals with the prediction of the performance of a real commercial PaT, numerically simulated in both direct and inverse mode, with an emphasis on the flow field through the impeller [21] (see Section 4). The proposed numerical investigation aims to put in evidence the slip phenomenon on a real configuration. The computational domain reproduces the entire geometry of the commercial pump, including the suction pipe, the impeller and the discharge pipe The introduction of a slip factor, $\sigma_{turbine}$, whose definition is equivalent to the one used for centrifugal pumps [22], accounts for the difference between the actual work and the theoretical one. This analysis is based on the evaluation of the axial and tangential velocities at the mean radius of the trailing edge of the blades at the outlet of the centripetal impeller. Moreover, this analysis shows the presence of different phenomena, e.g., pressure gradient and secondary flows, which may occur at the outlet of a centripetal turbine and affect the performance of the machine.

In the last part, a slip factor ($\sigma_{turbine}$) correlation has been derived from these numerical results. The definition of $\sigma_{turbine}$ provides a great support in developing and tuning 1-D models for the prediction of the turbine performance and it could provide the guidelines to successfully improve PaT geometries. A relationship between the new parameter ($\sigma_{turbine}$) and the flow rate is presented and discussed. This new correlation has been applied to the 1-D prediction model proposed by Stefanizzi et al. [22] in order to predict the entire characteristic of the same PaT, starting from the knowledge of its geometrical parameters. Finally, the same model has been applied to another real PaT with a similar specific speed (n_q) in order to compare the curve predicted by the model with the experimental one. In conclusion, the results of the new model show a more accurate prediction of the PaT performance under design and part-load conditions compared to the results of the same prediction models, employing slip factor correlations already available in the literature [23,24] (see Sections 5 and 6). The work focuses on a specific speed hydraulic turbomachinery; thus, it does not aim to be exhaustive—to cover the entire range of specific speeds, further analyses are required.

2. The Slip Phenomenon in Turbomachinery

As stated in the introduction, in turbines with a limited number of vanes, as in the case of PaT, a slip phenomenon occurs at the outlet section of the runner. The main effect of this phenomenon is related to the reduction of the Euler's work, Y, due to the flow deflection increasing the kinematic relative flow angle, β_1, with respect to the outlet congruent blade angle, β_{1B} (Figure 1). Unfortunately, there are few works in the literature that have investigated the effect of the slip phenomenon in power generating turbomachinery in detail—particularly in PaTs. Indeed, the evaluation of the slip effect is difficult, and there are not many experimental correlations.

Among the sources of the flow deflection, the vortex in the blade-to-blade plane (in particular in purely radial runners, as shown by Ventrone [19] and Shi et al. [20]) and the pressure gradient due to the blade loading together with the Coriolis force should be mentioned.

The flow inside the mixed axial-radial impeller is subjected to those complex phenomena; however, it is evident that the lower the number of blades, higher the blade loads, and hence the greater the flow deflection.

Figure 1 represents this phenomenon by showing both the actual (solid line) and the blade congruent velocity triangle (dashed line) at the runner outlet section. It is important to highlight that in this work, the subscripts 1 and 2 refer to the runner outlet and inlet, respectively. Moreover, all the quantities (pressure and velocities) will be considered as values averaged on the inlet and outlet areas. The flow deflection at the turbine outlet section 1 involves the increase of the tangential component

of the absolute velocity, c_{u1}, causing a decrease in terms of specific work, Y, obtained by the turbine, according to Euler's equation

$$Y = u_2 c_{u2} - u_1 c_{u1} \quad (1)$$

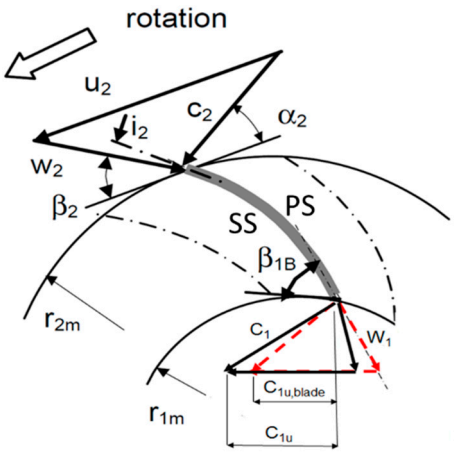

Figure 1. Velocity triangles at the inlet (2) and at the outlet of the runner (1). Both actual (solid line) and blade congruent (red dashed line) velocity triangles are represented at the outlet.

Neglecting secondary flows effects, the slip phenomenon at the outlet of mixed axial-radial runners is mainly due to the blade loading. Considering the flow at the PaT outlet (Figure 2) with tangential and meridional velocity components and no radial component, the fluid element, displayed in Figure 2, is subjected to a radial Coriolis acceleration, which does not contribute to modifying the pressure gradient along the tangential direction, but rather along the radial direction. Figure 2 schematically represents the acceleration terms in a qualitative way. Based on this representation, the Coriolis acceleration may introduce secondary flows, which will not be investigated in this work. Under these simplifications, the Coriolis acceleration does not influence the pressure gradient along the tangential direction; conversely, it is the main source of fluid flow deflection in centrifugal pumps.

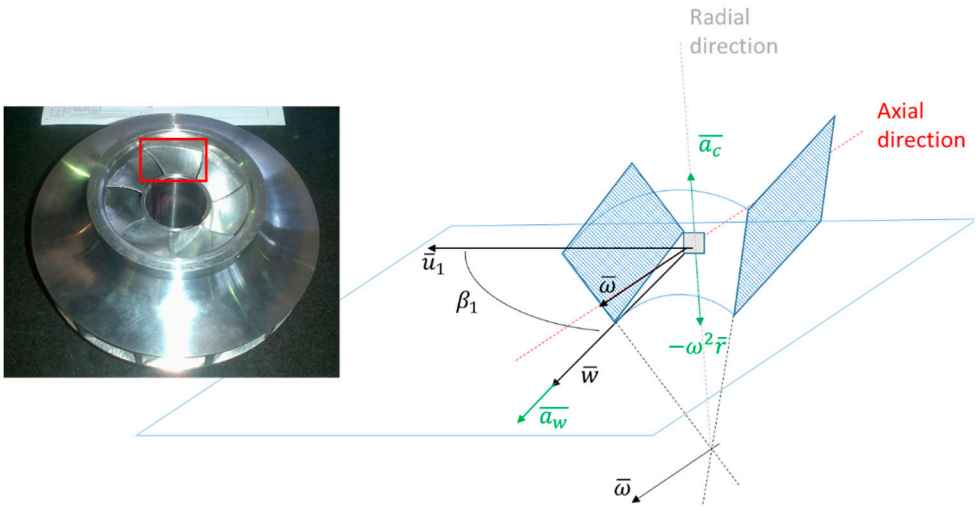

Figure 2. Representation of the main velocity vectors and accelerations referred to the particle of fluid at the outlet of the runner. The vector magnitudes are drawn qualitatively.

Although the above-mentioned works [19,20] have introduced the slip phenomenon in hydraulic turbines, it has often been neglected in the development of 1-D theoretical models, specifically in predicting PaT performance in turbine mode operation by taking into account the geometry of the

machine and some complex phenomena like hydraulic losses. Obviously, a deep insight into this phenomenon in real impellers could improve the accuracy of 1-D theoretical approaches in the performance prediction of pumps operating as turbines.

3. Influence of the Number of Blades on the Slip Phenomenon

In this section, an early-stage evaluation of the slip phenomenon is carried out by simulating a simplified archetype of a centrifugal pump vane by only changing the number of vanes (namely 6, 7 and 8) with the purpose of quantifying the effect of the pressure gradient acting in the tangential direction. This geometry does not consider the rounded trailing edge and its effects.

The simulation campaign was limited to single vanes (under the simplified hypothesis of periodic behavior). These geometries with different numbers of blades were designed by means of the model proposed by d'Agostino [25] and investigated by means of numerical simulations. The d'Agostino model expresses the 3D incompressible, inviscid, irrotational flow through helical blades with slow axial variations of the pitch and backsweep by superposing a 2D cross-sectional axial vorticity correction to a fully guided flow with axisymmetric stagnation velocity in the meridional plane. It is important to highlight that the three geometries have no blade thickness, since in this early stage of the slip phenomenon analysis, the rounded leading edges of the runner could complicate the investigation.

All the runners have the same specific speed, n_q = 20, and the value for the absolute tangential velocity calculated by means of the blade congruent theory at the center line (c_{line}) at the outlet of the impeller vane is $c_{u1} = 4.78$ m/s.

The specific speed is defined as

$$n_q = \frac{n\sqrt{Q_{BEP}/f_q}}{H^{0.75}} \tag{2}$$

where H is the hydraulic head (m), Q is the flow rate (m^3/s), n the rotational speed (rpm) and f_q is the number of impeller entries (f_q = 2 for a double suction impeller). The previous expression (Equation (2)) has been adopted to calculate both centrifugal pump and PaT specific speeds, since it is commonly used in empirical prediction model to forecast the BEP under turbine mode operation starting from the pump specific speed and vice versa.

Further geometric details are given in Table 1. The three single-vaned computational domains, designed according to d'Agostino, with a straight pipe at the inlet, are displayed in Figure 3.

Table 1. Geometric data about the centrifugal pump archetypes studied in this paragraph.

D_2 (mm)	l_2 (mm)	Z_{blades}	β_{2B} (°)	β_{1B} (°)	n (rpm)
252	12	6-7-8	17	25	3900

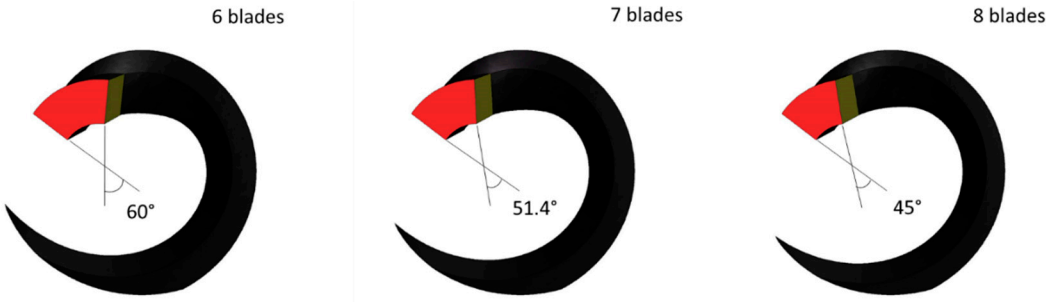

Figure 3. Three single vane geometries of the selected centrifugal pump with different number of blades.

The meshes were generated by means of Pointwise Gridgen® using unstructured tetrahedral elements. To guarantee the same grid density, a fixed node spacing has been applied to the connectors.

This means that the wider the vane (i.e., lower the number of blades), the larger the number of cells. The total number of cells for each geometry is reported in Table 2. The three computational domains are displayed in Figures 4 and 5, where their details at the inlet and outlet sections are shown.

Table 2. Number of cells of the centrifugal pump vane archetypes studied in this paragraph.

	6 Blades	7 Blades	8 Blades
Discharge pipe ($\times 10^6$)	0.46	0.40	0.34
Channel ($\times 10^6$)	0.80	0.70	0.60

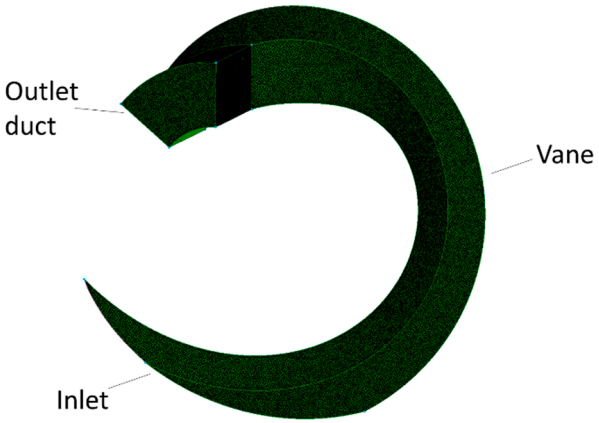

Figure 4. Grids of the single vane geometries with different number of blades.

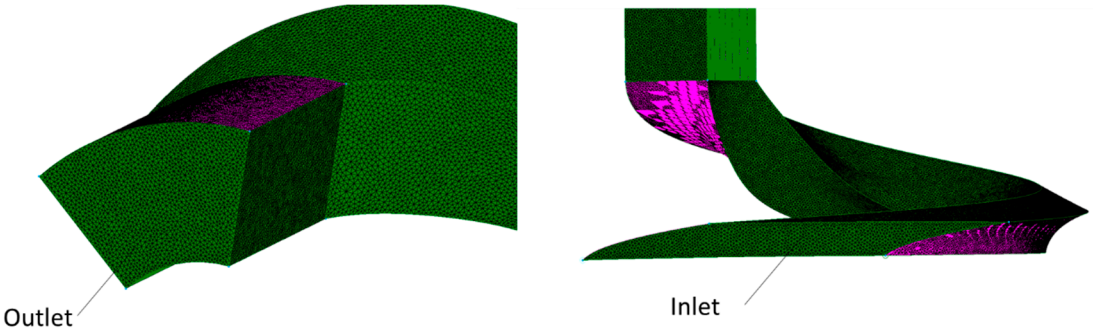

Figure 5. Grid details of the single vane geometry with 7 blades where the outlet and inlet section of the pump under turbine operating conditions are specified.

For this simplified case, simulations were run with the commercial CFD code ANSYS Fluent®, applying a single reference frame technique. In the next paragraph, when bigger meshes have to be analyzed, an open-source CFD code with no restriction on parallelization has been employed in order to reduce the computational time. With respect to the centrifugal pump the inlet and the outlet as well as the angular velocity have been reversed. At the inlet the absolute radial and tangential velocity components have been imposed with flow turbulent intensity equal to 3%, while uniform pressure was set up at the outlet. Due to the y^+ value calculated on the stator and rotor surfaces (y^+ =150), the k-ω SST model by Menter [26] with the application of the wall functions has been used for turbulence closure. This turbulence model is the standard for performing numerical analyses in hydraulic turbo machinery. It automatically uses the k-ω model in the near-wall regions, whereas the k-ε model is used away from the walls. The k-ω SST model can give an accurate prediction of flow separation, explaining its common use for the numerical investigations of flow inside the centrifugal pumps [27]. A zero shear stress has been applied to the walls belonging to the stator parts.

Evaluation of the Pressure and the Velocity Deflection

At the end of the simulation, the absolute tangential velocity (c_{u1}) and the static pressure were calculated at the outlet of the channel for the three geometries. The results were calculated along an arc at mean radius (0.0435 m), see Figure 6a and on iso-clips, see Figure 6b, in correspondence with the channel outlet section. As explained in Section 2, a flow deflection occurs at the outlet of the runner with respect to the blade congruent angle. Furthermore, considering that the higher the number of blades, the lower the blade loading, the pressure gradient at the outlet between the pressure and the suction side should be lower in the case with 8 blades than in the case with 6 blades. The p/p_{mean} ratio was plotted along an arc at the mean radius in correspondence of the vane outlet (z = 0 mm).

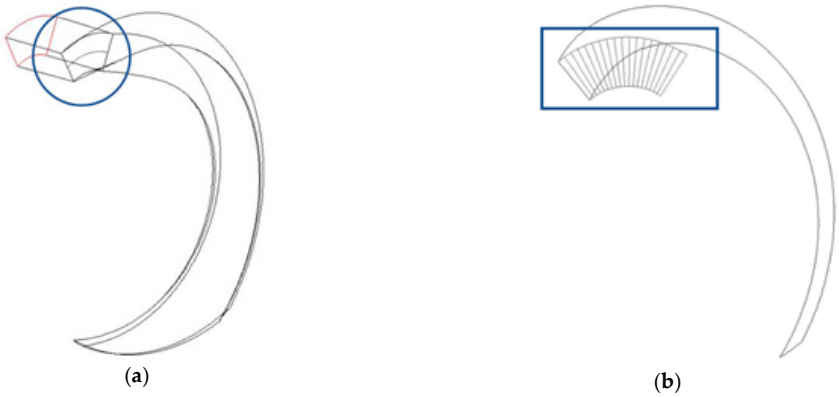

Figure 6. View of the arc (**a**) and the iso-clips (**b**) where the pressure and the velocity were evaluated.

Figure 7 points out that the higher the number of blades, the lower the pressure difference between the two sides of the blade. Moreover, the maximum p/p_{mean} value occurs for the impeller with 6 blades and all the maxima are placed roughly between 15 and 35% of each arc from the pressure to the suction side.

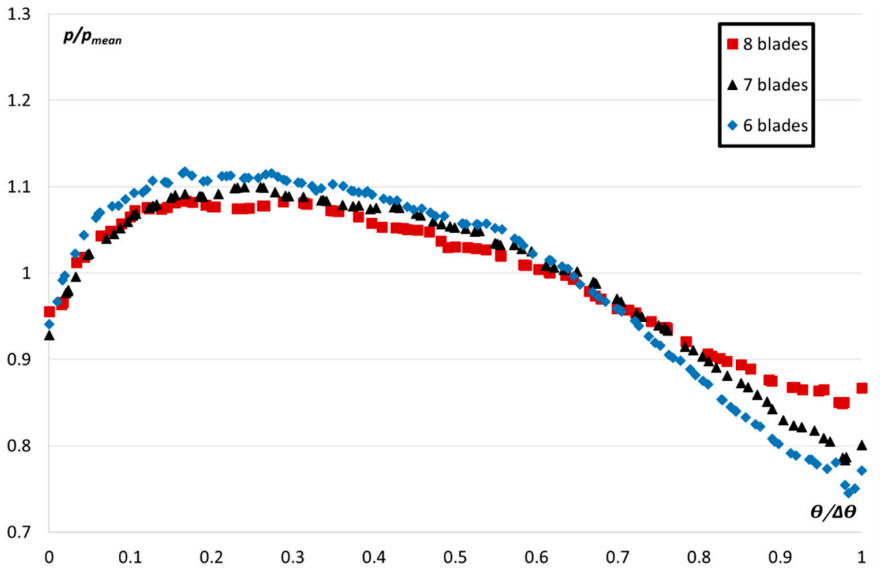

Figure 7. Pressure trends vs. the fraction of each arc from pressure side to suction side along the mean radius at the vane outlet of the three geometries.

Table 3 highlights the increase of the pressure difference between pressure and suction side with the decrease in the number of blades. These values were calculated from the previous Figure 7, as the difference between the extreme ends of the arcs.

Table 3. Pressure difference, Δp, between pressure and suction side of the blades for the three geometries with different number of blades and n_q equal to 20.

	6 Blades	7 Blades	8 Blades
Δp (Pa)	10,500	9000	6050
$\sigma_{turbine}$	0.947	0.951	0.953

After that, the velocity profiles were plotted on a dimensionless axis indicating the fraction of each arc from the pressure side to the suction side, where $\Delta\theta = 360° / Z_{blades}$; specifically, the velocities refer to the blade congruent absolute tangential velocity, $c_{u1,th}$. By comparing their trends, the maximum deflection occurs towards 30% of the arc, and this increases by decreasing the number of blades, see Figure 8.

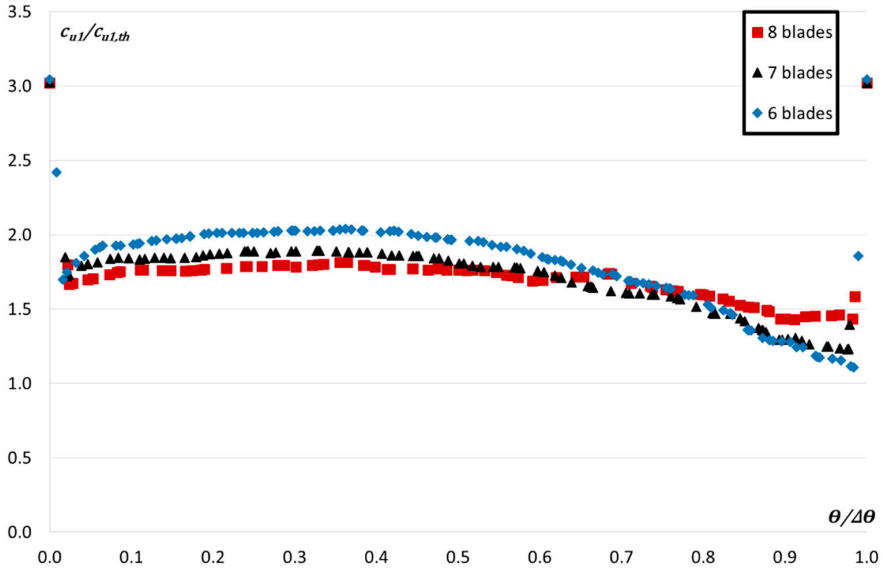

Figure 8. Absolute tangential velocity calculated via CFD (c_{u1}) over the blade congruent value for the three geometries ($c_{u1,th}$).

These results are coherent with the trend of the static pressure at the outlet of the vane (Figure 7). The 6 blades geometry shows steep variations close to the blades which leads to deflections up to +100% compared to the blade congruent value; on the other hand, the 8 blades geometry is subjected to smooth excursions and it displays a flat profile. To describe the flow deflection at the outlet of a centripetal hydraulic turbo machine, the slip factor, $\sigma_{turbine}$, has here been defined as the specific work calculated via CFD, Y_{CFD}, over the theoretical specific work, $Y_{1D,th}$

$$\sigma_{turbine} = \frac{Y_{CFD}}{Y_{1D,th}} \tag{3}$$

The results obtained by applying Equation (3) are summed up in Table 3, where it is evident that the slip factor decreases with the reduction of the number of blades. Hence, it can be stated that the higher the number of the blades, the better the flow guidance at the exit of the vanes (Figure 8); this guarantees lower losses and greater work extraction by the runner.

Moreover, the value of the absolute tangential velocity was evaluated on iso-clips (Figure 6b) by means of the following expression

$$c_{u1} = \frac{\iint (c_u u)\rho \bar{c} \Delta \overline{dA}}{G u_1} \tag{4}$$

where G is the ideal mass flow rate (kg/s) that flows through each iso-clip in Figure 6b. This calculation allows the evaluation of the variation of the absolute tangential velocity moving tangentially from pressure side ($\theta/\Delta\theta = 0$) to suction side ($\theta/\Delta\theta = 1$), see Figure 9. In this case, the velocity component is weighted by the mass flow rate, which actually flows through each iso-clip.

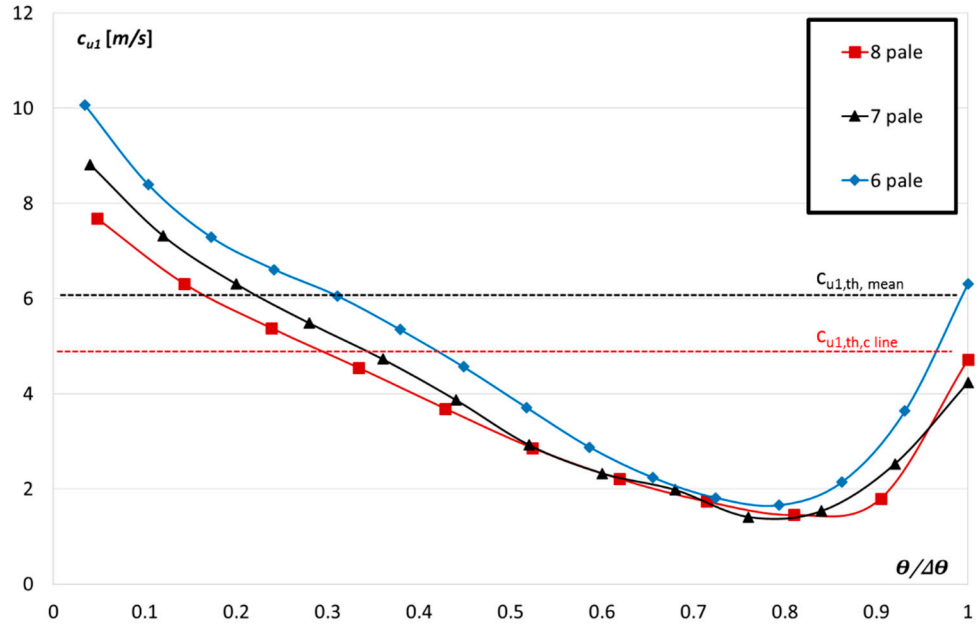

Figure 9. Trend of the absolute tangential velocity calculated on the iso-clips with Equation (4). $c_{u1,th,mean} = 6.03$ m/s, $c_{u1,th,\ c\ line} = 4.77$ m/s.

In this calculation, the results are influenced by the distribution of the flow rate, which is not homogeneous. Indeed, due to the Coriolis force, $\overline{F}_{coriolis} = 2m\overline{w} \times \overline{\omega}$, the mass flow rate is thickened close to the hub.

The meridional velocity over the theoretical value at the outlet of the vane is displayed in Figure 10. In conclusion, pressure gradients along the tangential and radial direction and secondary flows due to the Coriolis effect occur at the vane exit. These, together with the blade loading, promote the flow deflection at the outlet of the vane.

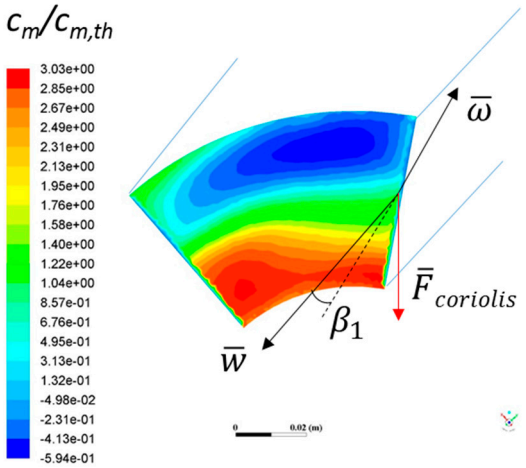

Figure 10. Contours of the meridional velocity over the theoretical value and representation of the Coriolis force and its effect at the outlet of the vane.

A local reversed flow (negative velocity) can be evidenced across the outlet of the vane and the inlet of the draft tube, as depicted by the velocity contours on the meridional plane (see Figure 11).

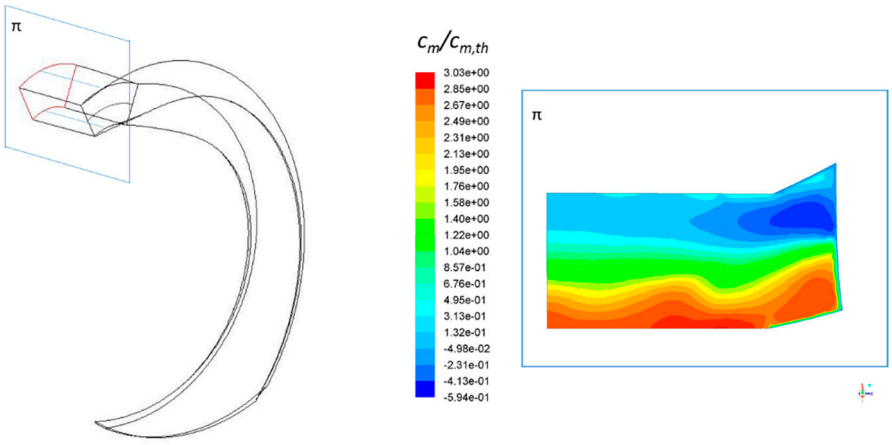

Figure 11. Contours of the meridional velocity over the theoretical value on a meridional plane, across the vane outlet and the initial part of the draft tube.

4. Numerical Study of a Real PaT

After the evaluation of the slip phenomenon at the outlet of the runners with no blade thickness, numerical investigations of a real double suction centrifugal pump have been carried out with the open-source CFD code OpenFOAM by solving the 3D U-RANS equations. The unsteady RANS equations were considered adequate to model the flow through the pump, where quantities have to be considered averaged over a time period short enough with respect to global unsteady phenomena but long enough for statistical significance. The transient simulations were run with an OpenFOAM application, pimpleDyMFoam, which is able to run transient simulations, including moving meshes, with incompressible flow. This application is based on the PIMPLE algorithm: a combination of the PISO (Pressure Implicit with Splitting of Operator) and SIMPLE (Semi-Implicit Method for Pressure-Linked Equations). The turbulence model applied for the system closure is the *k-ω* SST by Menter et al. [26].

This procedure has been validated in the past against experimental data of a double suction centrifugal pump [28].

4.1. Numerical Domain and Boundary Conditions

The geometry of a commercial pump with a specific speed $n_q \cong 21$ was simulated in both direct (pump) and inverse mode (turbine). The numerical domain studied in this work is represented in Figure 12. It includes the suction pipe, the impeller and the discharge pipe. Herein, the impeller investigated is a double suction impeller, actually two single suction centrifugal pump impellers with seven blades in a back-to-back configuration. This kind of centrifugal pump is employed to minimize the net positive suction head required when operating in pump mode. Moreover, the volute is doubled to balance the radial loads on the rotor and allow high-speed operation, also at part load [18]. The characteristic curve, see Figure 13, of the pump was calculated by means of unsteady simulations. The methodologies and the results have been deeply described by Capurso et. al. [21].

For all the analyzed cases, the mass flow rate has been imposed at the inlet considering a uniform inlet velocity distribution and a constant turbulent intensity equal to 3%. Moreover, the value of the mass flow leakage, which flows through the annular seal, has been modeled as exiting from the impeller case and incoming axially upstream the impeller eye with a 45° of swirl with respect to the tangential direction. The leakage was calculated a priori according to a one-dimensional empirical model because the geometry of the seal has not been included in the computational domain [21].

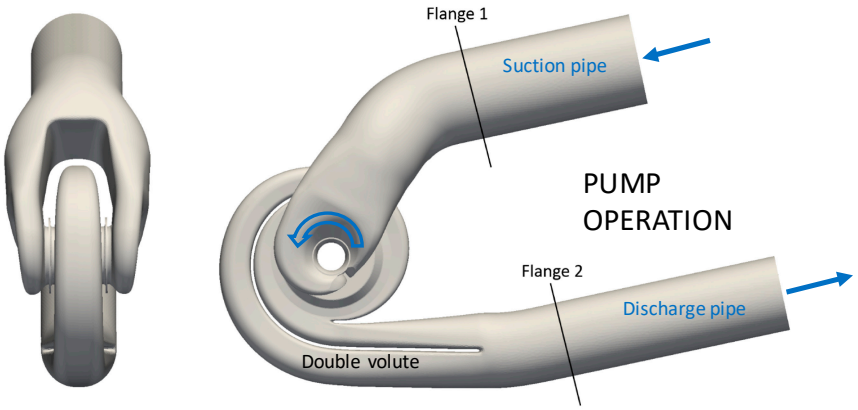

Figure 12. Front and side view of the CAD representing the centrifugal pump; the areas of Flange 1 and 2 were equal to 0.02840 m^2 and 0.01941 m^2, respectively.

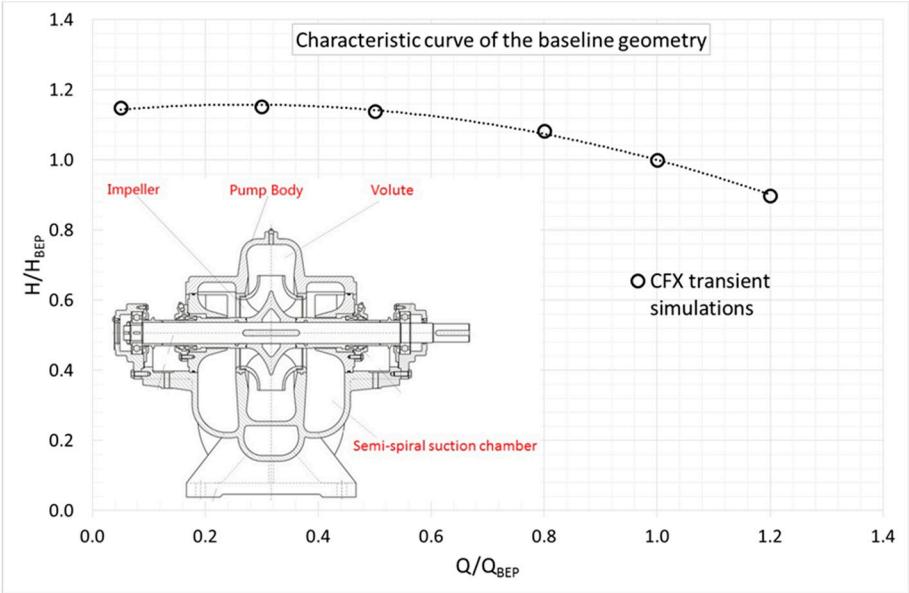

Figure 13. Characteristic curve of the commercial pump calculated by means of numerical simulations with CFX and 40 million of cells.

A uniform pressure distribution was imposed at the outlet of the domain. Straight pipes were added at the inlet and the outlet to extend the numerical domain in order to reduce uncertainties due to boundary conditions. The three parts of the geometry, which were merged together, communicate with each other by means of interfaces. In OpenFOAM, the boundary condition used on these interfaces is named cyclicAMI (i.e., Cyclic Arbitrary Mesh Interface).

An important feature is the wall roughness; indeed, different values of the equivalent sand grain roughness have been imposed to the stator (5.6×10^{-5} m) and the rotor surfaces (5.6×10^{-6} m). These values are typical values measured on real impellers manufactured for experimental test [29]. Further details about grid refinement study and boundary conditions employed for the numerical simulations are described in a previous work [21]. The results shown in the following paragraphs were calculated on a grid made of 11 million cells, represented in Figure 14.

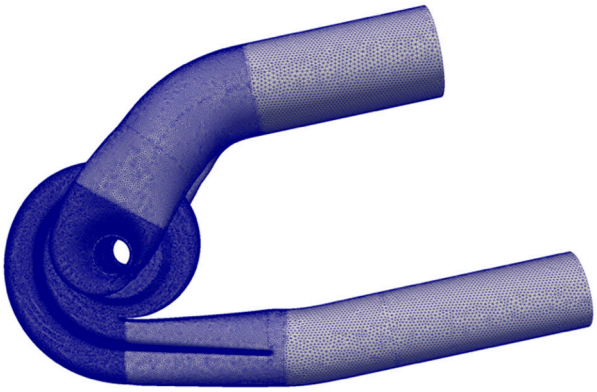

Figure 14. Front and side view of the CAD representing the centrifugal pump; the areas of Flange 1 and 2 were equal to 0.02840 m^2 and 0.01941 m^2, respectively.

4.2. Pump Mode Operation

The numerical set up has been assessed in a previous work [21] by comparing the results obtained with OpenFOAM and the consolidated commercial CFD code CFX. These results show a fairly good agreement with each other, as already experienced by Nilsson [30].

All the transient flow simulations were carried out with a time $\Delta t = T/(256\ Z_{blades}) = 4.5 \times 10^{-6}$ s, where T is the time period of a complete rotation and $Z_{blades} = 7$ is the number of blades, for a time lapse equal to 0.085 s, which corresponds to five complete impeller revolutions. The results in terms of head and efficiency were averaged over the last 3 revolutions. The mean and the maximum values of the Courant number have been approximately equal to 0.03 and 6, respectively, in all the simulations.

The numerically obtained characteristic curves of the impeller working either in pump (see Figure 12) or in turbine mode (see Figure 15) are represented on the same diagram with dimensionless axes (H/H_{BEP} vs Q/Q_{BEP}) in Figure 16, where H_{BEP} and Q_{BEP} are the head and the flow rate at the BEP of the pump, respectively. For completeness, $H_{BEP,P}/H_{BEP,T}$ and $Q_{BEP,P}/Q_{BEP,T}$ are equal to 0.958 and 0.832, respectively.

The head, H (m), is evaluated as follows

$$H = \frac{P_{tot_2} - P_{tot_1}}{\rho g} \tag{5}$$

where P_{tot} is the total pressure (N/m^2), the subscripts 1 and 2 correspond to the inlet and outlet flanges, see Figure 1, whereas the efficiency, η, is defined as

$$\eta_P = \frac{\Delta P_{tot} Q}{C\omega} \tag{6}$$

where the total pressure variation is $P_{tot,2} - P_{tot,1}$, C is the torque (Nm) resulting from the forces acting on the blades, hub and shroud of the impeller, comprising the disk friction losses, and ω is the rotational speed (rad/s).

4.3. Turbine Mode Operation

Eventually, a campaign of simulations was carried out with the machine operated in reverse mode applying the same setup previously described for the pump mode. However, the flow direction and the rotation of the impeller were inverted, see Figure 15.

In this case, the efficiency, η_T, is defined as

$$\eta_T = \frac{C\omega}{\Delta P_{tot} Q} \tag{7}$$

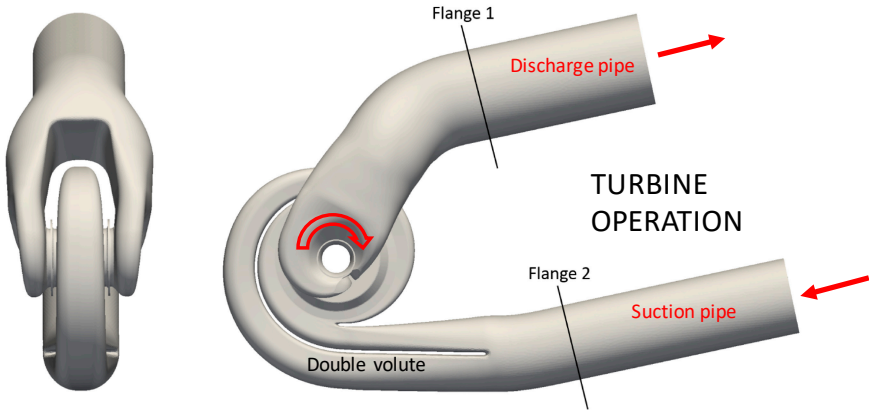

Figure 15. Numerical domain with the turbine operating conditions.

It is worth highlighting that no geometry modifications were applied to the impeller working in reverse mode, as usually happens in the reality, where the trailing edge of the blades are rounded to reduce the flow incidence losses. Generally, pumps operated as turbines work with a higher mass flow rate than when they are operated in direct mode. Therefore, numerical simulations were performed starting from $Q_{min}/Q_{BEP,P}$ equal to 70%, which is a value close to the runaway curve calculated according to the empirical model proposed by Gülich [18] (see Figure 16a), to $Q_{max}/Q_{BEP,P}$ equal to 140%. The maximum flow rate allows us to identify the BEP of the turbine (see Figure 16b). The mass flow leakages were calculated by means of the same equations provided by Gülich [18] for centrifugal pumps. Applying this model, the volumetric efficiency (η_v) for a PaT results constant at various flow rate.

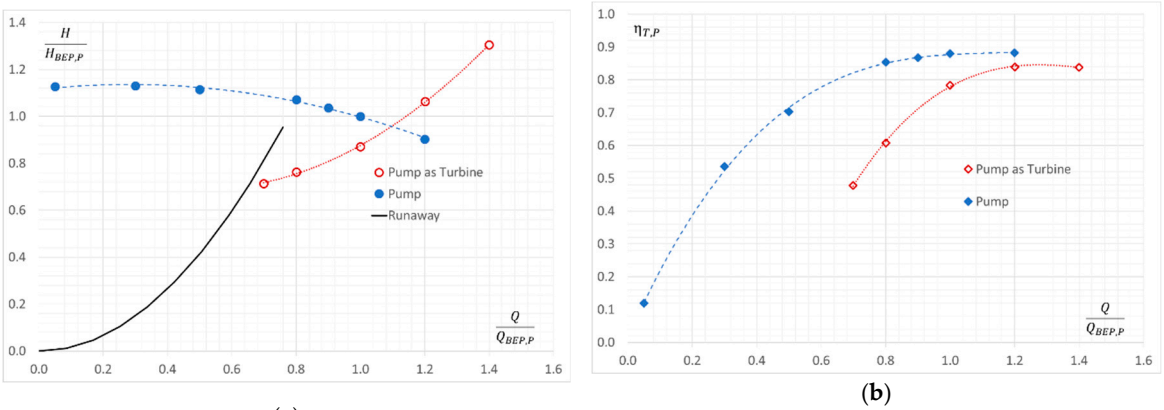

(**a**) (**b**)

Figure 16. Plot of the hydraulic turbo machine performance in both pump and turbine operating modes: (**a**) head curves calculated with Equation (5) with runaway curve; (**b**) Efficiency calculated with Equations (6) and (7).

4.4. Evaluation of the Velocity at the Outlet of the Runner

Actually, the main flow is subject to a deflection in the same direction of the machine rotation, which could be justified by different sources as explained in Sections 2 and 3, e.g., the vorticity inside the channel and the pressure gradient. This deflection leads to a reduction of the work extracted by the runner according to specific work equation (Equation (1)).

With the aim of quantifying this phenomenon, using the results of the numerical simulations, absolute tangential and axial velocity components were evaluated in Section 1, see Figure 1, by means of area-weighted averages on surfaces downstream the impeller exit. These values were time-averaged over the last 3 rotations of the machine. The mean value of the absolute tangential velocity is 4.40 m/s. This value has been compared with the theoretical value [21] computed at the

same flow rate, congruently with the blade angle at the outlet of the impeller (β_{1B}). For the machine studied in this work, the theoretical tangential velocity, calculated by means of the blade congruent flow theory at the BEP of the turbine, is equal to 2.08 m/s. Furthermore, the presence of the blades induces a strong and localized deflection of the flow field. It was noted that this might be justified by the tangential pressure gradient that occurs between pressure and suction side of the blades (see Figure 17). This is also shown in Figure 18, displaying the pressure along an arc at the mean radius.

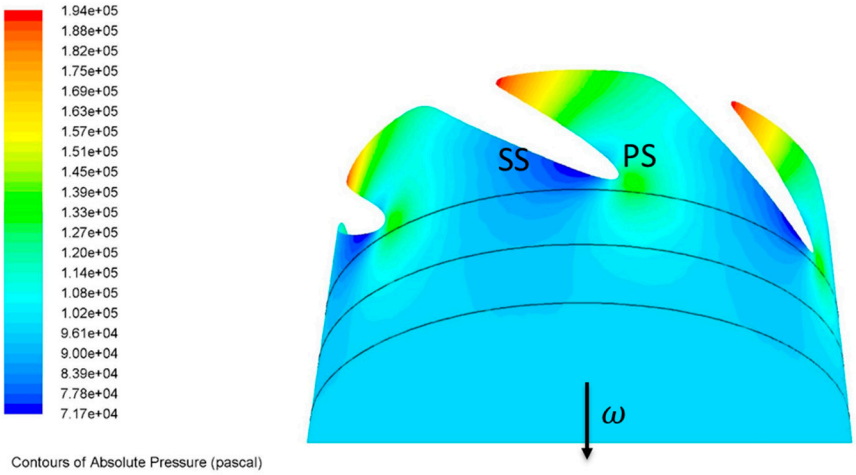

Figure 17. Contours of the static pressure (N/m^2) evidencing the pressure gradient across the blade trailing edge and at the mean radius.

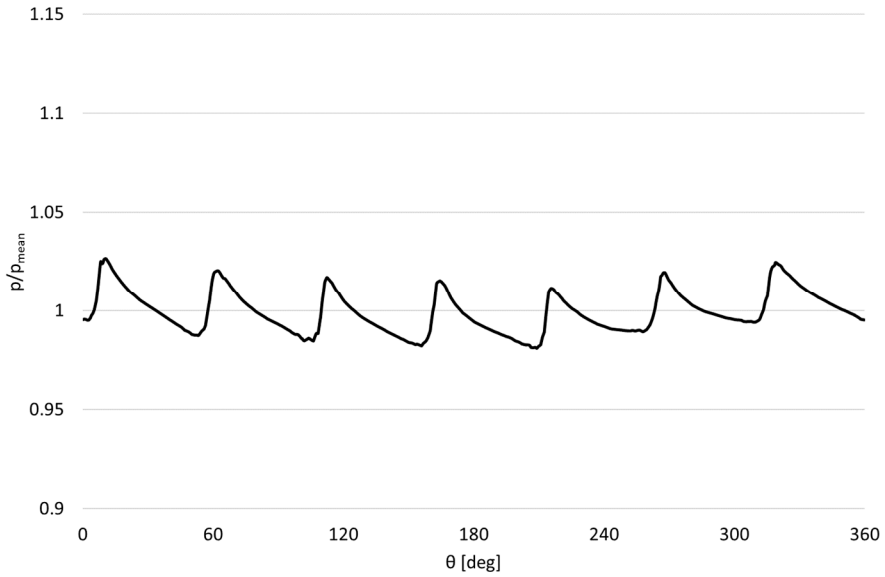

Figure 18. Pressure over the mean pressure (p/p_{mean}) along the mean radius at the trailing edge of the blade at the BEP.

To point out this contribution, axial and tangential velocity components were evaluated along the mean radius of the blades close to their trailing edge. The curve trends show a periodic behavior due to the presence of the blades (see Figure 19).

This means that the main flow at the outlet of the turbine is subject to a deflection not only due to the vortex inside the channel but also to the pressure gradient acting in the same direction. To further analyze the velocity vector components let's have a look at a short arc of the curve close to a blade to evaluate the tangential velocity component downstream of the runner.

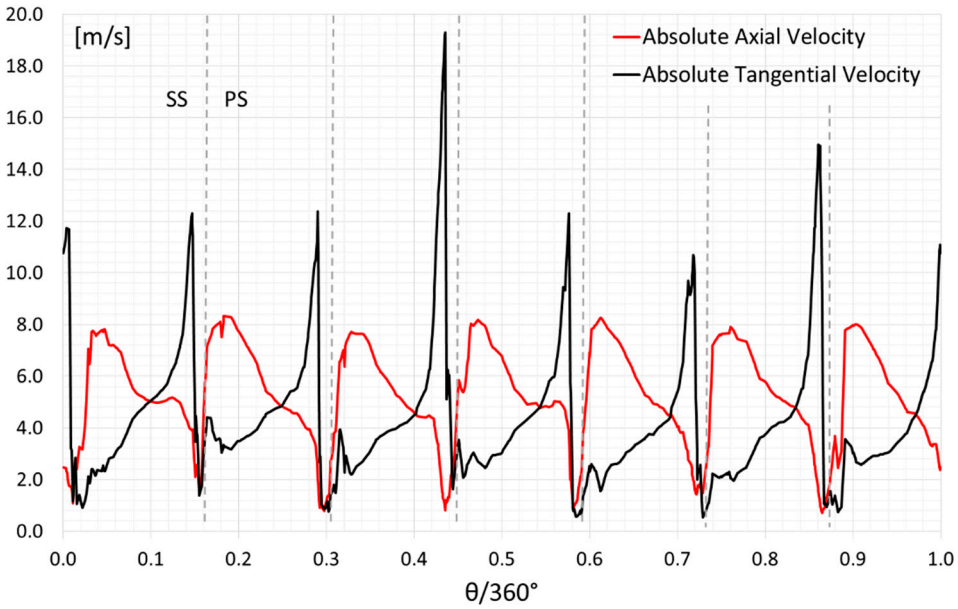

Figure 19. Representation of the axial and tangential components of the absolute velocity vector along the mean radius at the trailing edge of the blade (BEP operating point).

The tangential velocity was plotted on the same curve at different axial distance from the trailing edge (closer the curve, higher the peak). In proximity to the blade, there is a great increase of the tangential component due to the pressure gradient compared to the main flow, whereas towards the discharge, the velocity becomes more uniform and the peak gradually becomes smoother (see Figure 20).

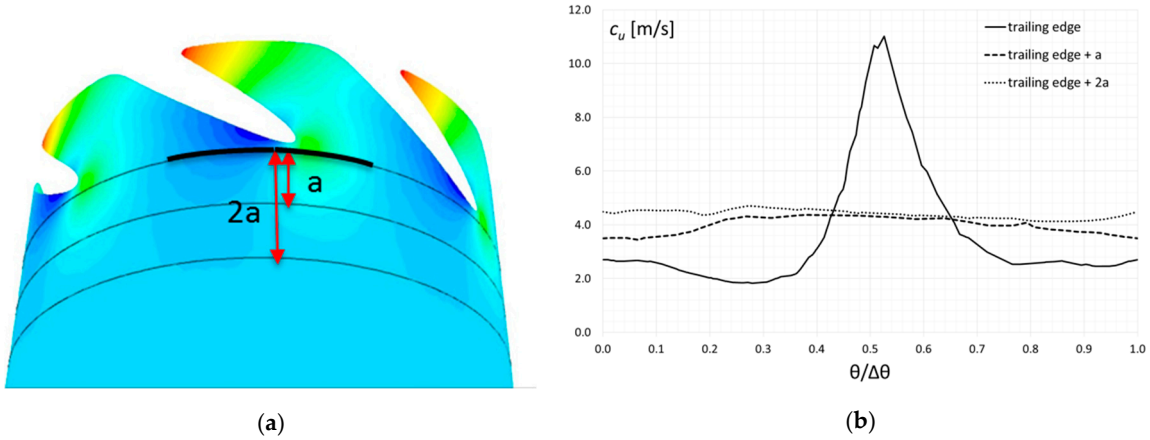

(**a**) (**b**)

Figure 20. Local analysis of the absolute tangential velocity distribution: (**a**) representation of an arc and three different distances from the trailing edge of the blade (0, +a, +2a); (**b**) absolute tangential velocity along an arc at three different distances at the mean radius at the trailing edge of the blade at the BEP.

The distances "a" = 0.5 cm and "2a" = 1 cm were chosen to be short enough to stay far from the influence of the curved suction elbow, but sufficiently close to the leading edge to investigate the area affected by the flow deflection.

As previously described, the slip factor gathers different sources of deflection, e.g., counter rotating vortex and pressure gradient at the trailing edge of the blade. Applying Euler's equation in order to compute the work both via 1-D theoretical model, $Y_{1D,th}$, and CFD calculi, Y_{CFD}, at the turbine BEP, the $\sigma_{turbine}$ is equal to 0.967.

Similarly to the theory of pumps where the slip factor corrects the ideal work transferred by the machine to the flow, the slip factor here introduced might be applied under turbine operating mode in order to correct the ideal work extracted by the PaT.

The slip factor was computed at different operating points, i.e., different mass flow rates, and the results are shown in Figure 21.

Then, a model of the slip factor was obtained by least-squares fitting, stated as follows

$$\sigma_{turbine} = 0.2365\left(\frac{Q}{Q_{BEP,P}}\right)^2 - 0.5537\left(\frac{Q}{Q_{BEP,P}}\right) + 1.2846 \quad (8)$$

Numerical simulations at different flow rates are suggested for the purpose of further exploring the slip factor behavior.

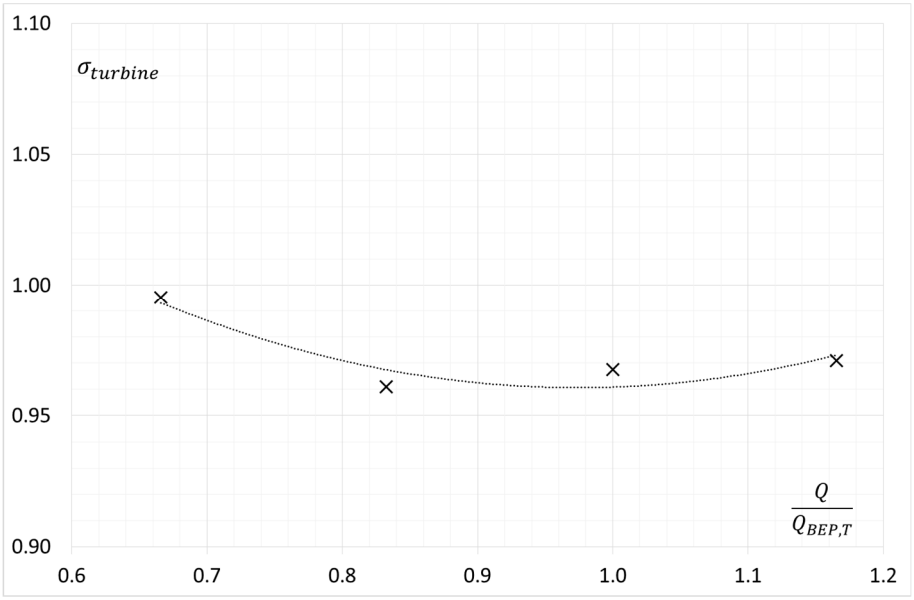

Figure 21. Slip factor in turbine mode, $\sigma_{turbine}$, vs flow rate ratio, $Q/Q_{BEP,T}$.

5. Theoretical 1-D Prediction Model

The results of numerical investigations were applied to a new 1-D model, which was previously developed by Stefanizzi et al. [22]. The work aims at adding the slip phenomenon effect in order to improve the model in terms of PaT performance prediction. The model is accurately described in [22] in order to predict the entire characteristic of a PaT, starting from the knowledge of its geometrical parameters and available related tests in turbine mode operation.

Figure 22 schematically illustrates how the model works: thanks to the knowledge of detailed geometrical data, flow rate, Q, and rotational speed, n, it is possible to accurately calculate the correct velocity triangles and the theoretical head, H_{th}, in reverse mode operation. Afterwards, volute ($Z_{volute,tot}$) and runner ($Z_{runner,tot}$) losses are modelled, whereas the theoretical head is reduced by means of the slip factor, $\sigma_{turbine}$, proposed in this paper. All these contributions are summed up to finally predict the real PaT head, $H_{turbine}$.

Some researchers, such as Barbarelli et al. [17] and Gülich [18], have developed theoretical approaches in order to predict PaT performance by taking into account velocity triangles, hydraulic losses on simplified geometries rather than using statistical and experimental correlations. However, the simplification of the geometry of impeller channel or volute could determine significant errors (±20%) in terms of performance prediction.

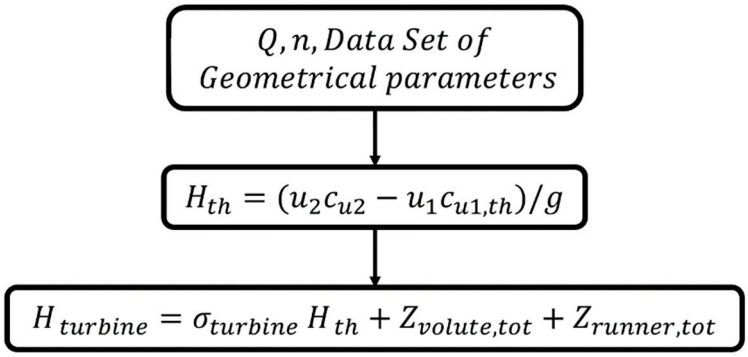

Figure 22. Flow chart of the 1-D proposed model.

5.1. Volute Losses

For the evaluation of volute losses, a generic double volute constituted by the inner and the outer volute has been considered and divided into three parts, as depicted in Figure 23: the inlet convergent channel (part 1), half volute collector (part 2) and the vane-less space between the throat volute section and the runner inlet section (part 3). As stated in Equation (9), the total volute head loss, $Z_{volute,tot}$, is obtained by summing up different contributes: (1) the head loss in the inlet convergent nozzle ($Z_{volute,1}$); (2) the volute loss in the collector ($Z_{volute,2}$); (3) the loss in the vaneless space ($Z_{volute,3}$).

$$Z_{volute,tot} = Z_{volute,a} = Z_{volute,b} = Z_{volute,1} + Z_{volute,2} + Z_{volute,3}. \quad (9)$$

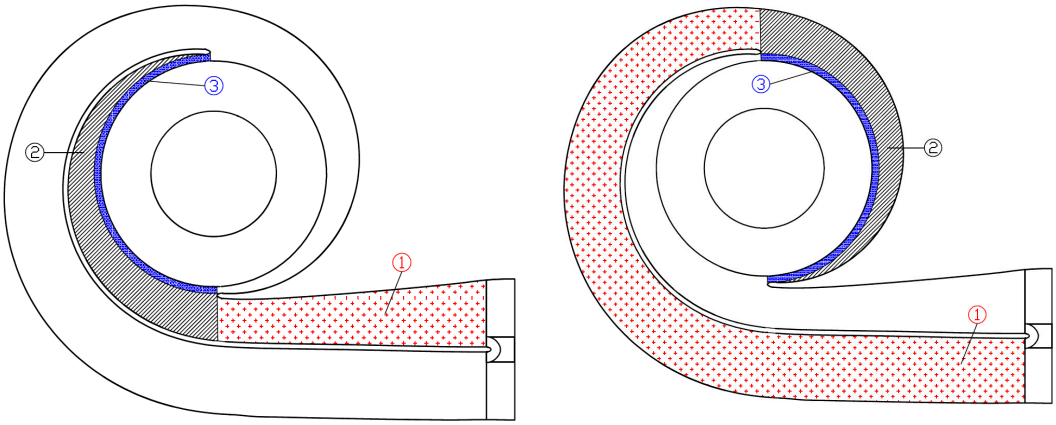

(**a**) (**b**)

Figure 23. Division of the double volute: inner volute (**a**) and outer volute (**b**).

5.2. Runner Losses

As stated in Equation (10), runner losses have different contributions. The first, $Z_{runner,1}$, is connected to the friction loss inside the impeller channel. Furthermore, with respect to Gülich's approach, the current model introduces new hydraulic parameters, as depicted in Figure 24. A flow incidence loss is contemplated at the inlet section of the runner, $Z_{runner,2}$, in order to take into account the difference between the inlet blade congruent angle, $\beta_{2,B}$, and the flow angle, β_2. Moreover, a blade blockage factor is used in order to consider the contraction of the inlet cross-area. This modifies the inlet velocity triangle, causing a loss due to the variation of the radial velocity component, $Z_{runner,3}$.

$$Z_{runner,tot} = Z_{runner,1} + Z_{runner,2} + Z_{runner,3} \quad (10)$$

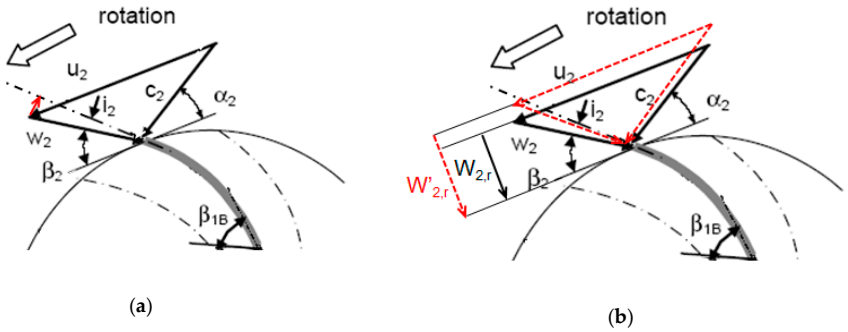

Figure 24. Runner losses: (**a**) the flow incidence loss; (**b**) variation of the radial component of the inlet relative velocity.

5.3. Application of the $\sigma_{turbine}$ Least-Square Fitting Curve to a 1-D Model

The 1-D model was applied to the machine numerically investigated in the previous Section 4. Figure 25 shows the comparison between the proposed model, Gülich's model and the current manufacturer's model used in the prediction of the characteristic curve during turbine mode. All predicted curves were compared with respect to that obtained by means of a numerical simulation performed by Capurso et al. [21].

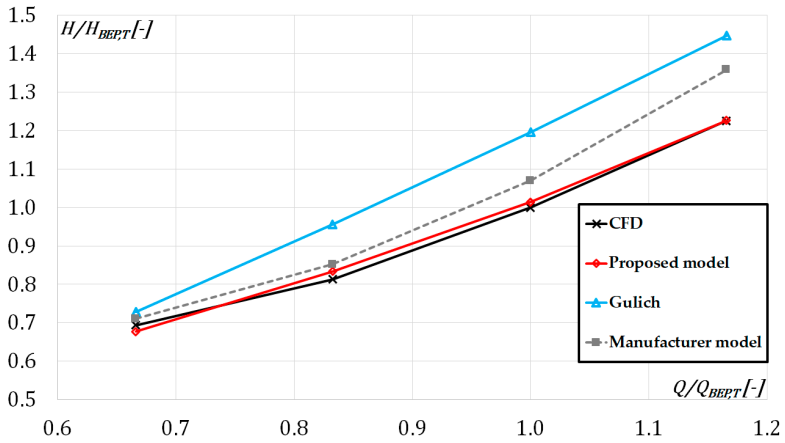

Figure 25. Comparison of different prediction models for the PaT characteristic curve.

As a result, the use of detailed geometrical information, the introduction of the slip factor and a new modelling of the hydraulic losses have determined a more accurate prediction of the PaT performance under design and off-design conditions. Indeed, the proposed 1-D model shows the best prediction at the lowest and the highest flow rates (respectively equal to −2.4% and 0.1%) with respect to Gülich's model (respectively equal to 5% and 18.1%) and to the manufacturer's model (respectively equal to 2.4% and 11%), as indicated in Table 4.

Table 4. Comparison of different prediction models for PaT characteristic curve in terms of head prediction errors.

$Q/Q_{BEP,T}$	0.67	0.82	1	1.17
Gülich	5.0%	17.5%	19.7%	18.1%
Proposed Model	−2.4%	2.6%	−1.5%	0.1%
Manufacturer	2.4%	4.8%	7.0%	11.0%

Figure 26 shows the contribution of each hydraulic loss considered in the proposed model in order to predict the characteristic curve obtained by CFD. The introduction of volute and runner losses causes an increasing of the turbine head, whereas the slip factor decreases the theoretical work calculated

by means of Euler's equation, and thus involves a better prediction for the different operating points. Furthermore, the flow incidence loss and the variation of the radial component of the relative inlet velocity show their remarkable contribution at lower flow rate.

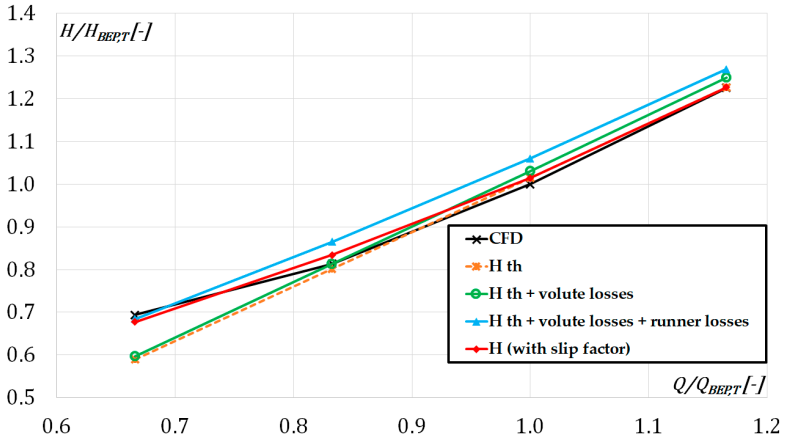

Figure 26. Comparison of different sources of losses for the performance prediction.

Moreover, three different slip factor definitions were applied to the 1-D model, as depicted in Figure 27. The results show that the model with the assumption that the slip factor term is negligible ($\sigma_{turbine} = 1$) overestimate the turbine head at the BEP with an error of 6.4%. On the other hand, both the Busemann [23] and Stodola [24] formulations applied to the 1-D model provide good results at the BEP, but underestimate the turbine head at part-loads, with an error of -8%. Instead, by applying the least-squares fitting of the CFD results, as described in Figures 21 and 26, errors are minimized over a wide range of flow rates.

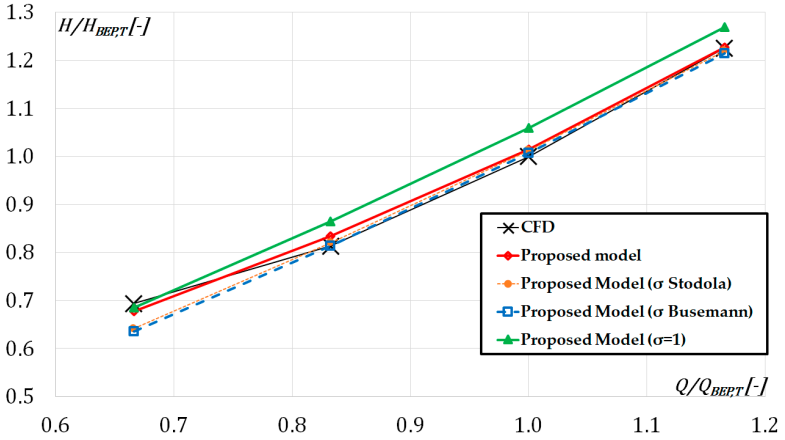

Figure 27. Comparison of different slip factor definitions (i.e., $\sigma_{turbine}$, σ proposed by Busemann [23], σ proposed by Stodola [24] and $\sigma = 1$) with the CFD results.

6. Experimental Case Study

To further assess the importance of including the slip phenomenon at the outlet of the runner, the model was applied to another double suction centrifugal pump, tested in both modes ($n_q = 26.46$, $D_2 = 432$ mm). In this case, the machine is characterized by a similar specific speed number, n_q, by the same number of blades and by similar outlet blade angle to those of the machine considered in Section 4. This means that the least-square fitting curve of (Equation (8)) can be also used for this machine. The proposed 1-D model has been applied to the machine by either considering or neglecting the slip factor. For the former case, two slip formulations have been considered: the slip factor evaluated by means of Equation (8) and the slip factor evaluated by Busemann. This comparison

is illustrated in Figure 28, where the predicted curves are compared with respect to the experimental one. The case without the slip phenomenon overestimates all the experimental operating points, whereas the case with the slip factor by Busemann underestimates them. Applying the proposed slip factor formulation, the model shows an intermediate behavior, resulting in a mean error lower than other cases, as summarized in Table 5. Obviously, the least-square fitting curve of Equation (8) was obtained thanks to numerical investigations on a single machine. Hence, further investigations need to be carried out in order to have a general applicability for machines characterized by different n_q, different numbers of blades, and outlet blade angles.

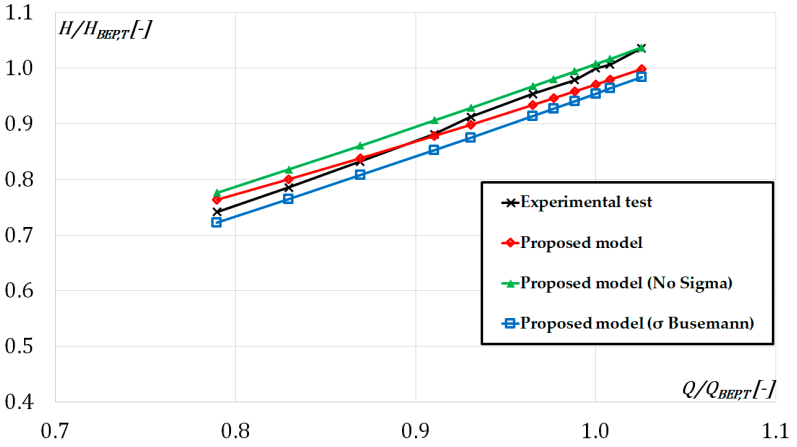

Figure 28. Comparison of different slip factor definitions in the 1-D curve prediction model (i.e., $\sigma_{turbine}$, σ proposed by Busemann and σ = 1) with the experimental curve.

Table 5. Comparison of different slip factor definition applied to the 1-D proposed prediction model for PaT characteristic curve in terms of head prediction errors.

$Q/Q_{BEP,T}$	**0.79**	**0.91**	**1**	**1.0**
Proposed Model (No sigma)	4.6%	2.8%	0.8%	0.1%
Proposed Model ($\sigma_{turbine}$)	2.9%	−0.4%	−2.9%	−3.7%
Proposed Model (σ Busemann)	−2.6%	−3.2%	−4.6%	−5.0%

7. Conclusions

This work shows numerical investigations of a centrifugal pump operating in reverse mode—namely, working as a turbine—with emphasis on the flow field at the runner outlet. Based on the results of these simulations, a correlation between slip factor and flow rate was introduced, improving the accuracy of a 1-D model for the prediction of PaT characteristic curves.

Firstly, possible sources of deflection of the flow at the outlet of PaT runners were discussed, according to the mechanism evidenced by Ventrone [19] and Shi et al. [20]. Given that the flow deflection at the runner outlet was associated with the finite number of blades, numerical investigations were carried out in order to quantify this effect. Thus, numerical analyses of simplified single vane geometries (no blade thickness and no rounded trailing edge influence) with different numbers of blades, designed with a potential flow tool, were performed. 3D steady-state simulations confirmed that lower the number of blades, higher the deflection.

After that, the flow field at the outlet of a commercial double suction centrifugal pump has been investigated by solving the 3D U-RANS equations through the entire machine. The presence of the slip phenomenon was pointed out by the evaluation of the tangential and axial absolute vectors components obtained via the numerical simulations. These results have been compared with the data resulting from the blade congruent flow theory. This analysis allowed the introduction of the slip factor, $\sigma_{turbine}$, which has been helpful in order to improve a 1-D model developed to predict the characteristic curve of a PaT starting from the pump geometry and its characteristic curves. Moreover,

a least-squares fitting curve, which describes the turbine slip factor, $\sigma_{turbine}$, at various flow rates, has been proposed by the authors. Indeed, the proposed 1-D model, including the slip factor correlation, shows good results over a wide range of mass flow rates, i.e., an improvement of the head prediction at the BEP (−5% error compared to no-slip, $\sigma = 1 = const$, 1-D models) and at part-load (−8% error) compared to the σ correlations proposed by Stodola [23] and Busemann [24].

In the future work, further investigations of a simplified geometry by varying its number of blade and its flow rate will be carried out in order to draw a map of the PaT slip factor, which could be useful for manufacturers.

Author Contributions: T.C. and M.S. wrote the paper; T.C. performed CFD analysis and M.S. developed the 1-D prediction model; G.P., M.T. and S.R. co-operated with T.C. and M.S. on the theoretical aspects concerning this topic. M.T., S.M.C. and B.F. supervised the work.

Funding: This research received no external funding.

Acknowledgments: The authors gratefully acknowledge Nuovo Pignone for their experimental support. During the review process of this article, we were saddened by the death of our colleague and friend, Bernardo Fortunato, who was one of the co-authors of this paper. Bernardo passed away on 31 January 2019, at the age of 68. Full professor at the age of 36, he was a preeminent researcher at the Polytechnic of Bari, serving it in several academic roles and as a responsible of research projects, always promoting studies on renewable energies. He supported and encouraged us in carrying out activities in the field of hydraulic pumps and PaTs, which underlie this paper. We had the pleasure and the honor to work with him and we hope to continue his work despite of his absence.

Conflicts of Interest: The authors declare no conflict of interest.

Abbreviations

BEP	Best Efficiency Point
CFD	Computational Fluid Dynamic
MHP	Micro Hydropower Plant
PaT	Pump as Turbine
WDN	Water Distribution Network

Nomenclature

a_c	[m/s^2]	Coriolis acceleration
a_w	[m/s^2]	Relative acceleration
C	[Nm]	Torque
c	[m/s]	Absolute velocity
D	[m]	Diameter
f_q	[-]	Number of impeller entries
G	[kg/s]	Mass flow rate
g	[m/s^2]	Gravitational acceleration
H	[m]	Head
l	[m]	Blade height
n	[rpm]	Rotational speed
n_q	[-]	Specific speed number (n in rpm, Q in m^3/s and H in m)
p	[Pa]	Pressure
Q	[m^3/s]	Flow rate
r	[m]	Radius
u	[m/s]	Tangential velocity
w	[m/s]	Relative velocity
Y	[J/kg]	Specific work
Z_{blades}	[-]	Number of blades
Z_{runner}	[m]	Volute loss
Z_{volute}	[m]	Runner loss

Greek Symbols

α	[rad]	Absolute flow angle
β	[rad]	Relative flow angle
η	[-]	Efficiency
θ	[rad]	Angular coordinate
ρ	[kg/m^3]	Density
σ	[-]	Slip factor
ω	[rad/s]	Angular velocity

Subscripts and Superscripts

1	Outlet section of the runner
2	Inlet section of the runner
B	Blade
m	Velocity meridional component
P	Pump
T	Turbine
th	Theoretical
u	Velocity tangential component
tot	Total

References

1. Laux, C.H. Reverse-running pumps as energy recovery turbines. *Sulzer Tech. Rep.* **1982**, *2*, 23–27.
2. Apfelbacher, R.; Etzold, F. Energy-Saving, Shock-Free Throttling with the Aid of a Reverse Running Centrifugal Pump. *KSB Tech. Rep.* **1988**, *24e*, 33–41.
3. Binama, M.; Su, W.T.; Li, X.B.; Li, F.C.; Wei, X.Z.; An, Z. Investigation on pump as turbine (PAT) technical aspects for micro hydropower schemes: A state-of-the-art review. *Renew. Sustain. Energy Rev.* **2017**, *79*, 148–179. [CrossRef]
4. Barbarelli, S.; Amelio, M.; Florio, G. Experimental activity at test rig validating correlations to select pumps running as turbines in microhydro plants. *Energy Conversion and Management* **2017**, *107*, 781–797. [CrossRef]
5. Derakhshan, S.; Nourbakhsh, A. Experimental study of characteristic curves of centrifugal pumps working as turbines in different specific speeds. *Exp. Therm. Fluid Sci.* **2008**, *32*, 800–807. [CrossRef]
6. Nautiyal, H.; Kumar, A.; Yadav, S. Experimental investigation of centrifugal pump working as turbine for small hydropower systems. *Energy Sci. Technol.* **2011**, *1*, 79–86.
7. Pugliese, F.; De Paola, F.; Fontana, N.; Giugni, M.; Marini, G. Experimental characterization of two Pumps as Turbines for hydropower generation. *Renew. Energy* **2016**, *99*, 180–187. [CrossRef]
8. Rossi, M.; Righetti, M.; Renzi, M. Pump-as-Turbine for energy recovery applications: The case study of an aqueduct. *Energy Procedia* **2016**, *101*, 1207–1214. [CrossRef]
9. Singh, P.; Nestmann, F. An optimization routine on prediction and selection model for the turbine operation of centrifugal pumps. *Exp. Therm. Fluid Sci.* **2010**, *34*, 152–164. [CrossRef]
10. Shi, G.; Liu, X.; Wang, Z.; Liu, Y. Conversion relation of centrifugal pumps as hydraulic turbines based on the amplification coefficient. *Adv. Mech. Eng.* **2017**, *9*, 1–8. [CrossRef]
11. Yang, S.S.; Derakhshan, S.; Kong, F.Y. Theoretical, numerical and experimental prediction of pump as turbine performance. *Renew. Energy* **2012**, *48*, 507–513. [CrossRef]
12. Tan, X.; Engeda, A. Performance of centrifugal pumps running in reverse as turbine: Part II—Systematic specific speed and specific diameter based performance prediction. *Renew. Energy* **2016**, *99*, 188–197. [CrossRef]
13. Carravetta, A.; Fecarotta, O.; Ramos, H.M. A new low-cost installation scheme of PATs for pico-hydropower to recover energy in residential areas. *Renew. Energy* **2018**, *125*, 1003–1014. [CrossRef]
14. Balacco, G. Performance Prediction of a Pump as Turbine Sensitivity Analysis Based on Artificial Neural Networks and Evolutionary Polynomial Regression. *Energies* **2018**, *11*, 3497. [CrossRef]

15. Rossi, M.; Renzi, M. A general methodology for performance prediction of Pumps-as-Turbines using Artificial Neural Networks. *Renew. Energy* **2018**, *128*, 265–274. [CrossRef]
16. Stefanizzi, M.; Torresi, M.; Fortunato, B.; Camporeale, S.M. Experimental investigation and performance prediction modeling of a single stage centrifugal pump operating as turbine. *Energy Procedia* **2017**, *126*, 589–596. [CrossRef]
17. Barbarelli, S.; Amelio, M.; Florio, G. Predictive model estimating the performance of centrifugal pumps used as turbines. *Energy* **2016**, *107*, 103–121. [CrossRef]
18. Gülich, J.F. *Centrifugal Pumps*, 2nd ed.; Springer: Berlin, Germany, 2008.
19. Ventrone, G. Deviazione della corrente relative nelle giranti delle turbine Francis. *L'Energia Elettr.* **1972**, *9*, 569–574.
20. Shi, G.; Liu, X.; Yang, J.; Miao, S.; Li, J. Theoretical research of hydraulic turbine performance based on slip factor within centripetal impeller. *Adv. Mech. Eng.* **2015**, 7. [CrossRef]
21. Capurso, T.; Stefanizzi, M.; Torresi, M.; Pascazio, G.; Caramia, G.; Camporeale, S.M.; Fortunato, B.; Bergamini, L. How to improve the Performance Prediction of a Pump as Turbine by Considering the Slip Phenomenon. *Proceedings* **2018**, *2*, 683. [CrossRef]
22. Stefanizzi, M.; Capurso, T.; Torresi, M.; Pascazio, G.; Ranaldo, S.; Camporeale, S.M.; Fortunato, B.; Monteriso, R. Development of a 1-D prediction model of a PaT performance under design and off-design conditions. *Proceedings* **2018**, *2*, 682. [CrossRef]
23. Busemann, A. Das Forderhohenverhaltnis Radialer Kreiselpumpen mit Logarithmisch-Spiraligen Schaufeln. *ZAMM J. Appl. Math. Mech.* **1928**, *8*, 372–384. [CrossRef]
24. Stodola, A. *Dampf und Gasturbinen*; Springer: Berlin, Germany, 1924.
25. D'Agostino, L.; Pasini, A.; Valentini, D. A reduced order model for preliminary design and performance prediction of radial turbopumps. In Proceedings of the 47th AIAA/ASME/SAE/ASEE Joint Propulsion Conference & Exhibit, San Diego, CA, USA, 31 July–3 August 2011. [CrossRef]
26. Menter, F.R.; Kuntz, M.; Langtry, R. Ten Years of Industrial Experience with the SST Turbulence Model. *Turbul. Heat Mass Transf.* **2003**, *4*, 625–632.
27. Huang, P.; Bardina, J.; Coakley, T. *Turbulence Modeling Validation, Testing, and Development*; NASA Technical Memorandum; NASA Ames Research Center: Moffett Field, CA, USA, 1997; Volume 110446.
28. Capurso, T.; Torresi, M.; Bergamini, L. Design and CFD performance analysis of a novel impeller for double suction centrifugal pumps. *Nuclear Eng. Design* **2018**, *341*, 155–166. [CrossRef]
29. Adams, T.; Grant, C.; Watson, H. A Simple Algorithm to Relate Measured Surface Roughness to Equivalent Sand-grain Roughness. *Int. J. Mech. Eng. Mechatron.* **2012**, *1*, 66–71. [CrossRef]
30. Nilsson, H. Evaluation of OpenFOAM for CFD of turbulent flow in water turbines. In Proceedings of the 23rd IAHR Symposium, Yokohama, Japan, 17–21 October 2006.